J. Plasma Physics (2009), *vol.* 75, *part* 1, *pp.* 91–98.
doi:10.1017/S0022377808007332 Printed in the United Kingdom

A mechanism for self-generated magnetic fields in the interaction of ultra-intense laser pulses with thin plasma targets

A. ABUDUREXITI[1,2], T. OKADA[2] and S. ISHIKAWA[2]

[1] Physics Department, Xinjiang University, Urumqi, 830046, People's Republic of China

[2] Faculty of Technology, Tokyo University of Agriculture and Technology, Koganei-shi, Tokyo, 184-8588, Japan
(okada@cc.tuat.ac.jp)

(Received 23 January 2008, accepted in revised form 15 April 2008, first published online 23 June 2008)

Abstract. In the study of the interaction of ultra-intense laser pulses with thin plasma targets there appears self-generated magnetic fields in the plasma target. The strong magnetic fields were directly measured in the plasma target, and were attributed to a mechanism of non-parallel electron temperature and density gradients. These magnetic fields can become strong enough to significantly affect the plasma transport. The underlying mechanism of the self-generated magnetic fields in the ultra-intense laser–plasma interactions is presented by using a two-dimensional particle-in-cell simulation.

1. Introduction

Recent advancements on ultra-intense, short-pulse lasers have allowed for the exploration of many novel regimes in the field of laser–plasma interactions. Fast particles generated by laser–plasma interactions can be used in many applications, from manufacturing to medicine and even for the initiation of tabletop nuclear reactions. Energetic particle generation by the interaction of ultra-intense laser pulses with plasmas has been demonstrated in many previous studies [1–4]. Self-generated magnetic fields have also been reported [5–9] in laser–plasma interactions. Experimental measurements of the self-generated magnetic field during ultra-high intensity ($>10^{19}$ W cm^{-2}) interactions indicated the existence of peak fields between 340 MG and 460 MG at intensities in the range of 9×10^{19} W cm^{-2} [5]. Particle-in-cell (PIC) simulations indicate that spontaneous quasistatic magnetic fields may be produced in the plasma when an ultra-intense laser interacts with the plasma. Such a self-generated magnetic field exerts tremendous influence on inertial confinement fusion, particularly for energy absorption and energy transport [10]. We have also determined the saturated magnetic fields of the Weibel instability [11, 12] in ultra-intense laser–plasma interactions using the laser intensity and plasma density [9]. We have previously analyzed energetic proton acceleration and bunch generation by ultra-intense laser pulses on the surface of thin plasma targets [1]. Strong self-generated magnetic fields also appeared in the interaction of ultra-intense laser pulses with thin plasma targets. These magnetic fields affect the movement of the energetic protons.

This paper reports a mechanism for self-generated magnetic fields in the interaction of ultra-intense laser pulse with a thin plasma target, resulting from non-parallel electron temperature and density gradients by theory and PIC simulations.

2. Mechanism for self-generated magnetic fields

In the interaction of ultra-intense lasers with plasma, the electron momentum equation can be written as [7]

$$\frac{d\mathbf{p}_\mathrm{e}}{dt} = -e\mathbf{E} - \frac{e}{c}\mathbf{v}_\mathrm{e} \times \mathbf{B} - \frac{1}{n_\mathrm{e}}\nabla(n_\mathrm{e}T_\mathrm{e}) \tag{2.1}$$

where $d/dt = \partial/\partial t + \mathbf{v}_\mathrm{e} \cdot \nabla$, $\mathbf{p}_\mathrm{e} = m_\mathrm{e}(T_\mathrm{e})\gamma\mathbf{v}_\mathrm{e}$ is the relativistic momentum, $m_\mathrm{e}(T_\mathrm{e}) = m_0 G(\xi) \equiv m_0 K_3(\xi)/K_2(\xi)$, $\xi = m_0 c^2/T_\mathrm{e}$, $\gamma = (1 - v_\mathrm{e}^2/c^2)^{-1/2}$ is the relativistic gamma factor, m_e is the electron mass, m_0 is the rest mass of the electrons, e is the electron charge, T_e is the electron temperature, n_e is the electron number density, and K_n is the Macdonald function of nth order.

We separate all the field variables as sums of the slow- and fast-varying parts. Thus $\mathbf{v}_\mathrm{e} = \langle \mathbf{v}_e \rangle + \mathbf{v}_{ef}$, $\mathbf{E} = \langle \mathbf{E} \rangle + \mathbf{E}_f$, and $\mathbf{B} = \langle \mathbf{B} \rangle + \mathbf{B}_f$. The slow-varying component of (2.1) is written as

$$\frac{D\langle \mathbf{p}_\mathrm{e} \rangle}{Dt} = -e\langle \mathbf{E} \rangle - \frac{e}{c}\langle \mathbf{v}_\mathrm{e} \rangle \times \langle \mathbf{B} \rangle + \mathbf{F} - \frac{1}{n_\mathrm{e}}\nabla(n_\mathrm{e}T_\mathrm{e}), \tag{2.2}$$

$$\mathbf{F} = -c^2\nabla(\gamma m_\mathrm{e}(T_\mathrm{e})) + \frac{c^2}{\gamma}\nabla m_\mathrm{e}(T_\mathrm{e}), \tag{2.3}$$

$$\gamma = \left(1 + \frac{e^2A^2}{m_\mathrm{e}^2(T_\mathrm{e})c^4}\right)^{1/2}, \tag{2.4}$$

where $D/Dt = \partial/\partial t + \langle \mathbf{v}_\mathrm{e} \rangle \cdot \nabla$, $\mathbf{F}$ is the electron ponderomotive force, and A is the vector potential of the laser light.

The equation of the averaged electric and magnetic fields are given by Faraday's law and Ampère's law,

$$\nabla \times \langle \mathbf{E} \rangle = -\frac{1}{c}\frac{\partial \langle \mathbf{B} \rangle}{\partial t}, \tag{2.5}$$

$$\nabla \times \langle \mathbf{B} \rangle = \frac{4\pi en}{c}(\langle \mathbf{v}_\mathrm{i} \rangle - \langle \mathbf{v}_\mathrm{e} \rangle). \tag{2.6}$$

Here $n = n_\mathrm{e} = n_\mathrm{i}$ is the quasi-neutral plasma number density, and the mean velocity $\mathbf{v}_\mathrm{i}$ of the non-relativistic ion fluid is determined by

$$m_\mathrm{i}\frac{D\langle \mathbf{v}_\mathrm{i} \rangle}{Dt} = e\langle \mathbf{E} \rangle + \frac{e}{c}\langle \mathbf{v}_\mathrm{i} \rangle \times \langle \mathbf{B} \rangle - \frac{1}{n_\mathrm{i}}\nabla(n_\mathrm{i}T_\mathrm{i}) \tag{2.7}$$

where $D/Dt = \partial/\partial t + \langle \mathbf{v}_\mathrm{i} \rangle \cdot \nabla$, m_i is the ion mass, and the ponderomotive force acting on the ion fluid is ignored because it is smaller than the electron ponderomotive force.

We take the curl of (2.2), assuming that the inertial force is small in comparison with the ponderomotive force, and we use (2.5) and (2.6) to obtain

$$\frac{\partial \langle \mathbf{B} \rangle}{\partial t} = \frac{c}{4\pi e}\nabla \times \left(\langle \mathbf{B} \rangle \times \frac{\nabla \times \langle \mathbf{B} \rangle}{n_\mathrm{e}}\right) + \frac{c}{en_\mathrm{e}}\nabla T_\mathrm{e} \times \nabla n_\mathrm{e} + \frac{c^3}{e\gamma^2}\nabla m_\mathrm{e}(T_\mathrm{e}) \times \nabla\gamma \tag{2.8}$$

where the ions are assumed to be immobile.

https://doi.org/10.1017/S0022377808007332 Published online by Cambridge University Press

In (2.8), the source terms of the self-generated magnetic fields are the second term and the third term on the right-hand side of (2.8). We consider the second term on the right-hand side of (2.8) and we obtain

$$\frac{\partial \langle \mathbf{B}_1 \rangle}{\partial t} \equiv \frac{c}{en_\mathrm{e}} \nabla T_\mathrm{e} \times \nabla n_\mathrm{e}. \tag{2.9}$$

We obtain from (2.9) that

$$\langle |\mathbf{B}_1| \rangle \approx \left(\frac{1}{2\pi}\right)^2 \frac{\lambda_\mu^2}{l_T l_n} (\omega_\mathrm{L} t) \frac{T_\mathrm{e}}{m_0 c^2} \frac{m_0 \omega_\mathrm{L} c}{e} = \left(\frac{1}{2\pi}\right)^2 \frac{\lambda_\mu^2}{l_T l_n} (\omega_\mathrm{L} t) \frac{T_\mathrm{e}}{m_0 c^2} B_0 \tag{2.10}$$

where λ_μ is the laser wavelength in micrometers, ω_L is the laser angular frequency, $B_0 = m_0 \omega_\mathrm{L} c/e = 101$ MG and l_T, l_n are the characteristic scale lengths in micrometers of the temperature and density inhomogeneities, respectively.

In (2.10), the temperature T_e is obtained by balancing the pressure gradient and the relativistic ponderomotive force of the circularly polarized electromagnetic waves as [4, 13–16]

$$T_\mathrm{e} = m_0 c^2 (\sqrt{1 + \lambda_\mu^2 I_{18}/2.74} - 1) \tag{2.11}$$

where I_{18} is the laser intensity in units of 10^{18} W cm^{-2} and λ_μ is 1.06.

From (2.10) and (2.11), the magnetic field $\langle |\mathbf{B}_1| \rangle$ is given by

$$\langle |\mathbf{B}_1| \rangle \approx 1.53 \times 10^{-2} \frac{\lambda_\mu^3}{l_T l_n} (\omega_\mathrm{L} t) \sqrt{I_{18}} B_0 \tag{2.12}$$

where $I_{18} \gg 1$ [9].

Usually experiments and modeling are conducted with azimuthal symmetry with a focused laser beam propagating in the x-direction and interacting with a planar solid surface normal to the axis. The dominant component of ∇n_e is $(\partial n_\mathrm{e}/\partial x)\mathbf{x}$, the dominant component of ∇T_e is $(\partial T_\mathrm{e}/\partial y)\mathbf{y}$ and then the direction of the self-generated magnetic fields is in the z-direction.

3. Numerical simulation and discussion

In order to explain the mechanism of the self-generated magnetic field, we performed an electromagnetic PIC simulation. Simulations were performed for a laser with a wavelength λ_L of 1.06 μm, a laser pulse width of 40 fs, a laser beam diameter of 1.5 μm, and a laser intensity of 10^{20} W cm^{-2}. The laser pulse is linearly polarized, normally incident, and the intensity distribution has a Gaussian shape in space. We consider a circular concave target. The maximum electron density is $n_e = 4n_\mathrm{c}$, where n_c is the critical density. The initial temperature of electrons and ions is 1 keV and 0.8 keV, respectively, and the electron–ion mass ratio is 1/1836. The time step is chosen to be $0.1/\omega_\mathrm{L}$, and the spatial step is $0.3c/\omega_\mathrm{L}$. The gradient and constant plasma densities were in the ranges of 1.0 μm and 2.0 μm, respectively. In this simulation, the coordinate x is longitudinal and y is transverse. The laser pulse is in the x-direction. Periodic boundary conditions are applied in the transverse direction. We assume an absorbing boundary for the fields and a thermal reflection boundary for particle in the x-direction. The number of spatial grids in the plasma region and particles in the default parameter are $118\lambda_\mathrm{L} \times 17\lambda_\mathrm{L}$ and 7×10^5, respectively.

The geometry of the target containing the concave cavity [1] is shown in Fig. 1. In Fig. 2, the spatial distribution of the electron density from a circular concave target

https://doi.org/10.1017/S0022377808007332 Published online by Cambridge University Press

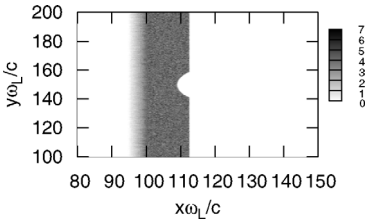

Figure 1. Geometry of the target containing the concave cavity.

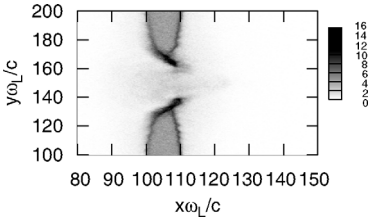

Figure 2. Spatial distribution of electron density from a circular concave target at $\omega_L t = 350$. The laser pulse ($I = 10^{20}$ W cm^{-2}) comes in from the left.

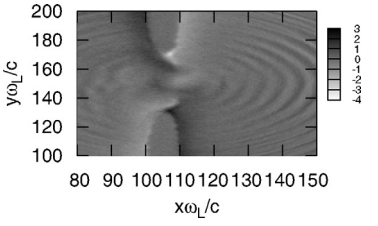

Figure 3. Spatial distribution of magnetic fields at $\omega_L t = 350$.

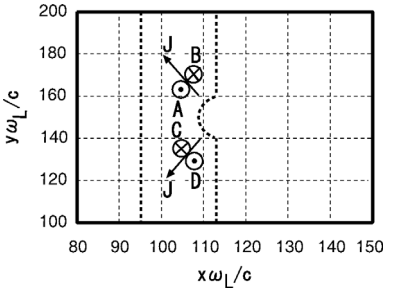

Figure 4. Schematic figure of the self-generated magnetic fields and currents J.

at $\omega_L t = 350$ is shown. In Fig. 3, the self-generated magnetic fields from a circular concave target for $I = 10^{20}$ W cm^{-2} at $\omega_L t = 350$ are shown. The schematic figure of the self-generated magnetic fields and currents is shown in Fig. 4. In Fig. 4, the lines $x\omega_L/c = 105$ and $y\omega_L/c = 165$, the lines $x\omega_L/c = 107$ and $y\omega_L/c = 170$, the lines $x\omega_L/c = 105$ and $y\omega_L/c = 135$, and the lines $x\omega_L/c = 107$ and $y\omega_L/c = 130$ cross at the point A, B, C, and D, respectively. In Fig. 5, the electron temperature

https://doi.org/10.1017/S0022377808007332 Published online by Cambridge University Press

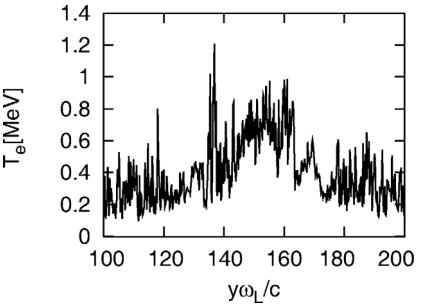

Figure 5. Temperature profile on the line $x\omega_{\mathrm{L}}/c = 105$ at $\omega_{\mathrm{L}}t = 350$.

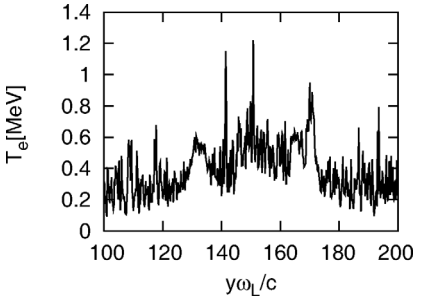

Figure 6. Temperature profile on the line $x\omega_{\mathrm{L}}/c = 107$ at $\omega_{\mathrm{L}}t = 350$.

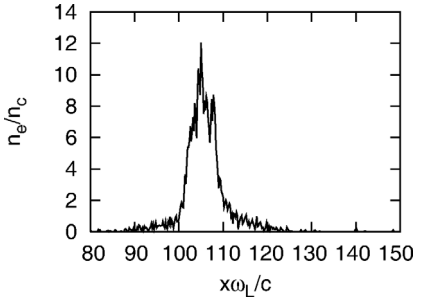

Figure 7. Density profile on the line $y\omega_{\mathrm{L}}/c = 130$ at $\omega_{\mathrm{L}}t = 350$.

is shown on the line $x\omega_{\mathrm{L}}/c = 105$ at $\omega_{\mathrm{L}}t = 350$. In Fig. 6, the electron temperature is shown on the line $x\omega_{\mathrm{L}}/c = 107$ at $\omega_{\mathrm{L}}t = 350$. In Fig. 7, the electron density is shown on the line $y\omega_{\mathrm{L}}/c = 130$ at $\omega_{\mathrm{L}}t = 350$. In Fig. 8, the electron density is shown on the line $y\omega_{\mathrm{L}}/c = 135$ at $\omega_{\mathrm{L}}t = 350$. In Fig. 9, the electron density is shown on the line $y\omega_{\mathrm{L}}/c = 165$ at $\omega_{\mathrm{L}}t = 350$. In Fig. 10, the electron density is shown on the line $y\omega_{\mathrm{L}}/c = 170$ at $\omega_{\mathrm{L}}t = 350$. The positive direction of the self-generated magnetic field on point A in Fig. 4 is explained by the mechanism of $\nabla T_{\mathrm{e}} \times \nabla n_{\mathrm{e}}$ by using Figs 5 and 9. The negative direction of the self-generated magnetic field on the point B in Fig. 4 is explained by the mechanism of $\nabla T_{\mathrm{e}} \times \nabla n_{\mathrm{e}}$ by using Figs 6 and 10. The negative direction of the self-generated magnetic field on the point C in Fig. 4 is explained by the mechanism of $\nabla T_{\mathrm{e}} \times \nabla n_{\mathrm{e}}$ by using Figs 5 and 8. The positive direction of the self-generated magnetic field on the point D in Fig. 4 is explained by the mechanism of $\nabla T_{\mathrm{e}} \times \nabla n_{\mathrm{e}}$ by using Figs 6 and 7. In Figs 11 and 12,

https://doi.org/10.1017/S0022377808007332 Published online by Cambridge University Press

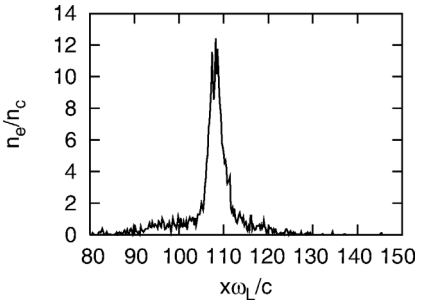

Figure 8. Density profile on the line $y\omega_L/c = 135$ at $\omega_L t = 350$.

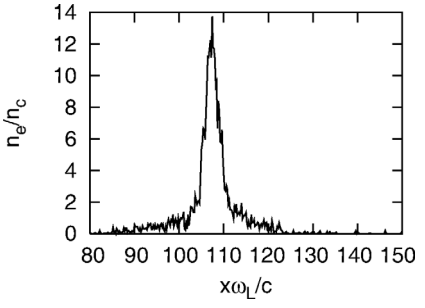

Figure 9. Density profile on the line $y\omega_L/c = 165$ at $\omega_L t = 350$.

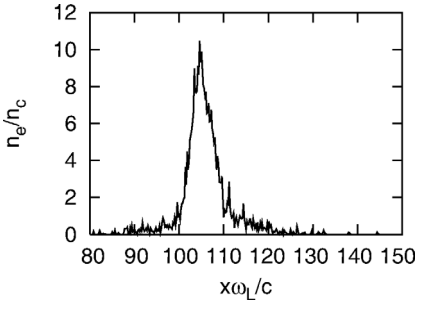

Figure 10. Density profile on the line $y\omega_L/c = 170$ at $\omega_L t = 350$.

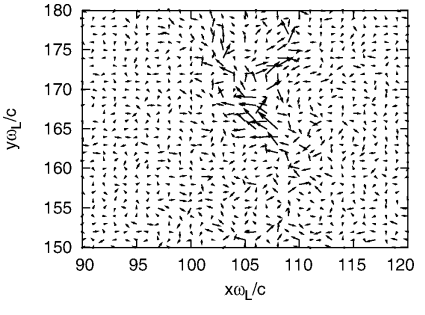

Figure 11. Distribution of the vectors of electric current density in the ranges $90 \leqslant x\omega_L/c \leqslant 120$ and $150 \leqslant y\omega_L/c \leqslant 180$ at $\omega_L t = 350$.

https://doi.org/10.1017/S0022377808007332 Published online by Cambridge University Press

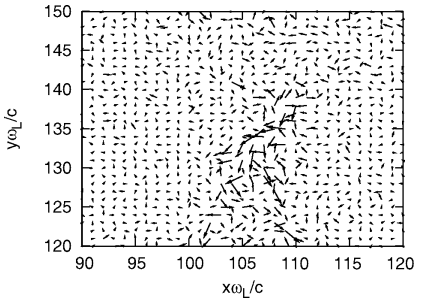

Figure 12. Distribution of the vectors of electric current density in the ranges $90 \leqslant x\omega_{\rm L}/c \leqslant 120$ and $120 \leqslant y\omega_{\rm L}/c \leqslant 150$ at $\omega_{\rm L}t = 350$.

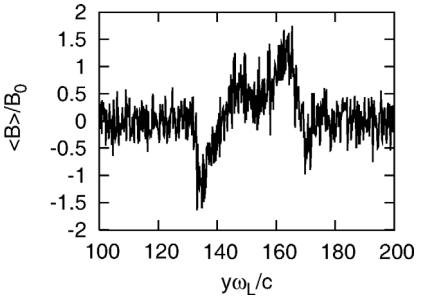

Figure 13. The self-generated magnetic fields on the line $x\omega_{\rm L}/c = 105$ at $\omega_{\rm L}t = 350$.

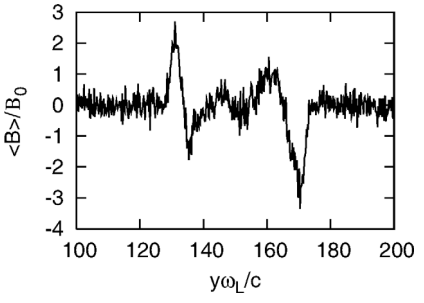

Figure 14. The self-generated magnetic fields on the line $x\omega_{\rm L}/c = 107$ at $\omega_{\rm L}t = 350$.

distributions of the vectors of electric current density are shown. In Figs 13 and 14, the self-generated magnetic fields are shown.

The self-generated magnetic field can be calculated using $l_T \approx l_n \approx 4$ (μm) which is estimated from Figs 5–10 and (2.12) to be $\langle|\mathbf{B}_1|\rangle = 403$ MG for $I = 10^{20}$ W cm^{-2}. From Fig. 14 we can estimate the peak value of the self-generated magnetic fields to be about $\langle B\rangle = 350$ MG for $I = 10^{20}$ W cm^{-2}. The self-generated magnetic field $\langle|\mathbf{B}_1|\rangle$ is consistent with $\langle B\rangle$.

https://doi.org/10.1017/S0022377808007332 Published online by Cambridge University Press

4. Conclusions

In the interaction of ultra-intense laser pulses with thin plasma targets there appeared strong self-generated magnetic fields in the plasma target. The self-generated magnetic fields were attributed to a mechanism of non-parallel electron temperature and density gradients. The spontaneously generated magnetic fields could significantly affect the propagation of laser-produced energetic plasmas.

Acknowledgements

This work was performed under the collaboration program of the Institute of Laser Engineering, Osaka University, Japan.

References

[1] Okada, T., Andreev, A. A., Mikado, Y. and Okubo, K. 2006 *Phys. Rev.* E **74**, 026401.
[2] Mackinon, A. J., Sentoku, Y., Patel, P. K., Price, D. W., Hatchett, S., Key, M. H., Andersen, C., Snavely, R. and Freeman, R. R. 2002 *Phys. Rev. Lett.* **88**, 215006.
[3] Sentoku, Y., Mima, K., Sheng, Z. M., Kaw, P., Nishihara, K. and Nishikawa, K. 2002 *Phys. Rev.* E **65**, 046408.
[4] Wilks, S. C., Langdon, A. B., Cowan, T. E., Roth, M., Singh, M., Hatchett, S., Key, M. H., Pennington, D., Mackinnon, A. and Snavely, R. A. 2001 *Phys. Plasmas* **8**, 542.
[5] Tatarakis, M., Gopal, A., Watts, I., Beg, F. N., Dangor, A. E., Kruselnick, K., Wagner, U., Norreys, P. A., Clark, E. L., Zepf, M. and Evans, R. G. 2002 *Phys. Plasmas* **9**, 2244.
[6] Haines, M. G. 1997 *Phys. Rev. Lett.* **78**, 254.
[7] Tsintsadze, L. N. and Shukla, P. K. 1994 *Phys. Lett.* A **187**, 67.
[8] Sudan, R. N. 1993 *Phys. Rev. Lett.* **70**, 3075.
[9] Okada, T. and Ogawa, K. 2007 *Phys. Plasmas* **14**, 072702.
[10] Sugie, M., Ogawa, K. and Okada, T. 2006 *Japan. J. Appl. Phys.* **45**, L1311.
[11] Weibel, E. S. 1959 *Phys. Rev. Lett.* **2**, 83.
[12] Okada, T., Yabe, T. and Niu, K. 1977 *J. Phys. Soc. Japan* **43**, 1042.
[13] Yu, M. Y. and Shukla, P. K. 1978 *Phys. Rev.* A **18**, 1591.
[14] Shukla, P. K., Yu, M. Y. and Tsintsadze, N. L. 1984 *Phys. Fluids* **27**, 327.
[15] Yu, M. Y., Shukla, P. K. and Tsintsadze, N. L. 1982 *Phys. Fluids* **25**, 1049.
[16] Shukla, P. K., Rao, N. N., Yu, M. Y. and Tsintsadze, N. L. 1986 *Phys. Rep.* **138**, 1.